Catalysis Today 157 (2010) 83–88

Contents lists available at ScienceDirect

Catalysis Today

journal homepage: www.elsevier.com/locate/cattod

Preferential CO oxidation in a H_2-rich gas by Au/CeO_2 catalysts: Nanoscale CeO_2 shape effect and mechanism aspect

Guangquan Yi [a], Hongwei Yang [a], Bodong Li [a], Haiqiang Lin [a], Ken-ichi Tanaka [b], Youzhu Yuan [a,*]

[a] State Key Laboratory of Physical Chemistry of Solid Surfaces, National Engineering Laboratory for Green Chemical Productions of Alcohols-Ethers-Esters, College of Chemistry and Chemical Engineering, Xiamen University, Xiamen 361005, PR China
[b] Advanced Science Research Laboratory, Saitama Institute of Technology, 1690 Fusaiji, Fukaya, Saitama 369-0293, Japan

ARTICLE INFO

Article history:
Available online 21 February 2010

Keywords:
Gold
CeO_2
CO preferential oxidation
Shape effect
Hydrogen isotope effect
Mechanism

ABSTRACT

The Au/CeO_2 catalysts with nanoscale CeO_2 shapes of rods, cubes and polyhedra were evaluated for the CO preferential oxidation (CO-PROX) in a hydrogen-rich gas, showing a strong effect of CeO_2 morphology followed by this order: rods > polyhedra > cubes. The results of pulse experiment and kinetic study indicated that the oxidation of CO could be enhanced by H_2 and H_2O moisture, behaving a hydrogen isotope effect by H_2/D_2. The catalyst Au/CeO_2-rods exhibited the lowest apparent activation energy for the CO oxidation either with or without hydrogen in comparison with the Au/CeO_2-polyhedra and Au/CeO_2-cubes. It was proposed that hydrogen reacted with adsorbed oxygen to yield highly oxidizing surface H-containing intermediates that could readily converted CO to CO_2 at lower temperatures. The generation of such key intermediates might be involved into the rate-determining step.

© 2010 Elsevier B.V. All rights reserved.

1. Introduction

The preferential oxidation of CO in a hydrogen-rich gas (CO-PROX) has been attracted much attention due to its unique role in purifying the gas feeding for proton-exchange-membrane (PEM) fuel cells [1–3]. Hydrogen produced after the steam reforming process and water-gas shift reaction usually contains trace amount of CO (0.5–1%) which will poison the platinum-based electrode that converts hydrogen to electricity [4]. The acceptable CO concentration is below 10 ppm at Pt anode and below 100 ppm at CO-tolerant alloy anodes. Among the approaches investigated to remove the trace amount of CO in H_2-rich stream [5,6], the CO-PROX has been considered to be suitable for sufficient CO removal.

Various efforts have been made with the development of CO-PROX catalysts by employing precious and non-precious metals. In particular, the supported noble metals, such as Au, Pt, Rh, Ru, and Ir were very active for this reaction [6–10]. Specifically, some selected metal oxides supported Au nanoparticles, were found to be of potentially superiority, since they are able to remove CO from reformed fuels with an extraordinarily high reaction rate and good selectivity at much lower temperatures [11–13]. The influence of metal oxides on the catalytic activity of gold nanoparticles has obtained great scientific interest. The active (reducible) supports such as TiO_2 [14–16], CeO_2 [13,17–19] and FeO_x [12,20–22] can improve the stability of gold particles and furnish oxygen atoms for higher activity. Interface, geometry, and quantum size effects determine the catalytic activity of gold nanoparticles supported on metal oxides.

CeO_2 is an attractive oxide with unique catalytic properties due to its distinct defect chemistry and the ability to exchange lattice oxygen with the gas phase [23]. These properties include the promotion of the precious metal dispersion, the enhancement of the catalytic activity at the interfacial metal-support sites and the promotion of CO removal through oxidation employing lattice oxygen. Nanosized gold supported on CeO_2 has been reported to be good catalyst in the CO-PROX in H_2 stream, owing to their high activity and selectivity to CO oxidation, and their resistance toward H_2O and CO_2 [13,17–19]. Quite recently, we have discovered that the catalytic activity of Au/CeO_2 on CO-PROX was significantly influenced by the morphology and crystalline planes of CeO_2 [24]. The nanoscaled Au supported on CeO_2 with the shape of rods exhibited extra higher activity than CeO_2 with the shapes of polyhedra and cubes.

On the other hand, even though numerous reports are available on the effect of metal oxide support on the activity of gold nanoparticles for the PROX reaction, there is less attention toward the CO-PROX reaction mechanism [19,22]. As for the total oxidation of CO, in general, the CO molecule is considered to be adsorbed on gold; the oxygen species activated on the surface of CeO_2 diffuse to the Au–CeO_2 interface and react with CO to produce CO_2 [25]. However, the CO-PROX reaction may not be described by such traditional mechanism. Concerning the hydrogen effect, Quinet et al. proposed that hydrogen reacted with oxygen to yield highly oxidizing intermediate HOO* that promoted CO oxidation

* Corresponding author. Tel.: +86 592 2181659; fax: +86 592 2183047.
E-mail address: yzyuan@xmu.edu.cn (Y. Yuan).

0920-5861/$ – see front matter © 2010 Elsevier B.V. All rights reserved.
doi:10.1016/j.cattod.2010.01.049

over Au/Al_2O_3 catalyst [26]. Recently, Tanaka et al. reported a novel catalyst $FeO_x/Pt/TiO_2$ and demonstrated that the PROX reaction of CO occurred *via* a HCOO intermediate and its oxidation with OH instead of oxygen, which was different from the ordinary oxidation of CO with O_2 [27].

The aim of this work is to further discuss the key issues relevant to the CeO_2 shape effect and mechanism aspects of the Au/CeO_2 catalysts for the CO-PROX by means of kinetic study, pulse experiment, effects of H_2/D_2 and water moisture. The results support the aforementioned morphology effect of CeO_2 and allow us to propose a H_2-promoted CO-PROX reaction mechanism.

2. Experimental

2.1. Catalyst preparation

Ceria oxides with shapes of rods, cubes and polyhedra were prepared by an established method [24,28]. The Au/CeO_2 catalysts with different shapes were prepared using a routine deposition–precipitation (DP) method described previously [29]. In brief, the CeO_2 samples were dispersed in aqueous solution of $HAuCl_4{\cdot}3H_2O$ at a pH of 8–9 using $(NH_4)_2CO_3$ as buffer solution. The precipitates were aged at room temperature and further washed with hot deionized water. Finally, the catalysts were obtained by calcination in air at 673 K for 4 h.

The nominal gold loading was controlled to be 1 wt%. The actual Au content was determined by an inductively coupled plasma-optical emission spectrometry (ICP-OES) using a Thermo Electron IRIS Intrepid II XSP. The received values were 0.92 wt% for the Au/CeO_2-rods, 0.83 wt% for the Au/CeO_2-polyhedra and 0.92 wt% for the Au/CeO_2-cubes.

2.2. Catalytic testing

The catalytic performances were examined in a conventional fixed-bed flow reactor by using 100 mg of catalyst at 0.1 MPa as previously reported [24]. The reactant mixture of $CO/O_2/H_2/N_2$ was adjusted to 1/1/50/48 (mol%) by mass flow controllers. The mixed gas passed through a tube containing NaOH pellets for purification. The typical performances were conducted at a total flow rate of 50 mL min^{-1}, corresponding to a gas hourly space velocity (GHSV) = 30,000 mL g^{-1} h^{-1}. The effect of CO_2 and H_2O co-existed in the feed gas was performed at the reactant mixture of 1% CO, 1% O_2, 50% H_2, 15% CO_2 and 10% H_2O balanced with N_2. The outlet stream line from the reactor to the gas chromatograph was heated at about 373 K to avoid condensation of reaction products. The composition of the influent and effluent gas was analyzed by an on-line gas chromatograph equipped with two packed columns (Molecular sieve 5A and Porapak Q) and thermal conductivity detector. The CO conversion and O_2 selectivity were calculated by the equations as previously reported [24].

The kinetic study was performed using different catalyst amounts (5 mg of Au/CeO_2-rods, 10 mg of Au/CeO_2-polyhedra and 50 mg of Au/CeO_2-cubes) in order to control the CO conversion below 20%. The flow rate of the reaction gas was maintained as 50 mL min^{-1}. The kinetic data were collected after the reaction for 30 min at each temperature when it attained a steady state.

2.3. Pulse experiment

Pulse experiments were performed on a lab-built microreactor equipped with a quadrupole mass spectrometer (Hiden Analytical) by using Ar as the carrier gas in a flow rate of 40 mL min^{-1}. The catalyst sample (20 mg) was pretreated at 523 K in $5\%O_2/95\%N_2$ flow for 30 min and then cooled down to 323 K. The sample was then purged with Ar 30 min at 323 K. After that, the amount of ca. 0.5 mL of $CO/H_2/Ar$ = 5/45/50 (mol%) or O_2/Ar = 20/80 (mol%) was pulsed into the catalyst bed at an interval of about 5 min. All the mixed gases were purified by the NaOH pellets before being pulsed into the catalyst bed. The effluent gas from the reactor was detected by the mass spectrometer by monitoring m/e = 28 for CO and m/e = 44 for CO_2.

2.4. Effects of hydrogen isotope and H_2O moisture

Hydrogen isotope effect and influence of water vapor were evaluated using the same reactor system as in the activity test by using 100 mg of catalyst at 0.1 MPa. Before D_2/H_2 or H_2O was introduced into the catalyst bed, the CO oxidation was executed from room temperature to 333 K with a reactant mixture of $CO/O_2/N_2$ (1/1/98, mol%) and then the temperature was held at 333 K. For the hydrogen isotope effect, D_2 (25 mL min^{-1}) or H_2 (25 mL min^{-1}) was added to a flow of $1\%CO + 1\%O_2$ balanced with N_2. The total flow rate was kept as 50 mL min^{-1}, where the N_2 flow rate was lowered from 49 to 24 mL min^{-1} when H_2 or D_2 (25 mL min^{-1}) was added. At each stage, the activity data was collected every 30 min after the reaction attained the steady state.

Effect of H_2O moisture on the CO oxidation was conducted by adding water vapor to the reactant mixture of $CO/O_2/N_2$ (1/1/98, mol%). The content of H_2O vapor was controlled by mixing dry N_2 with the N_2 bubbled through a water tank at room temperature, keeping the total flow rate at 50 mL min^{-1}.

2.5. High-resolution transmission electron microscopy

Transmission electron microscopy (TEM) images were performed on a Tecnai F30 electron microscope operated at an acceleration voltage of 300 kV. Samples for TEM measurements were ultrasonically dispersed in ethanol. Drops of suspensions were deposited on a copper grid coated with carbon.

3. Results and discussion

We have demonstrated the CO-PROX performance on the Au/CeO_2 catalysts with different CeO_2 shapes were dependent of CeO_2 morphology [24]. The CO-PROX performance over the same Au/CeO_2 ones with different shapes in the presence of CO_2 and H_2O vapor is displayed in Fig. 1. It can be seen that the Au/CeO_2-rods showed much higher activity than the Au/CeO_2-polyhedra and the Au/CeO_2-cubes in the temperatures ranging from 310 K to 393 K.

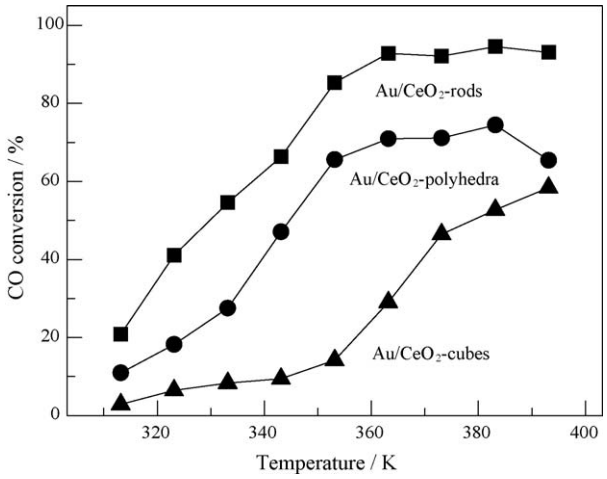

Fig. 1. Reaction temperature dependence of CO conversion over Au/CeO_2 with different CeO_2 shapes in the PROX reaction with a reactant mixture of 1% CO, 1% O_2, 50% H_2, 15% CO_2 and 10% H_2O balanced with N_2 under GHSV = 30,000 mL g^{-1} h^{-1}.

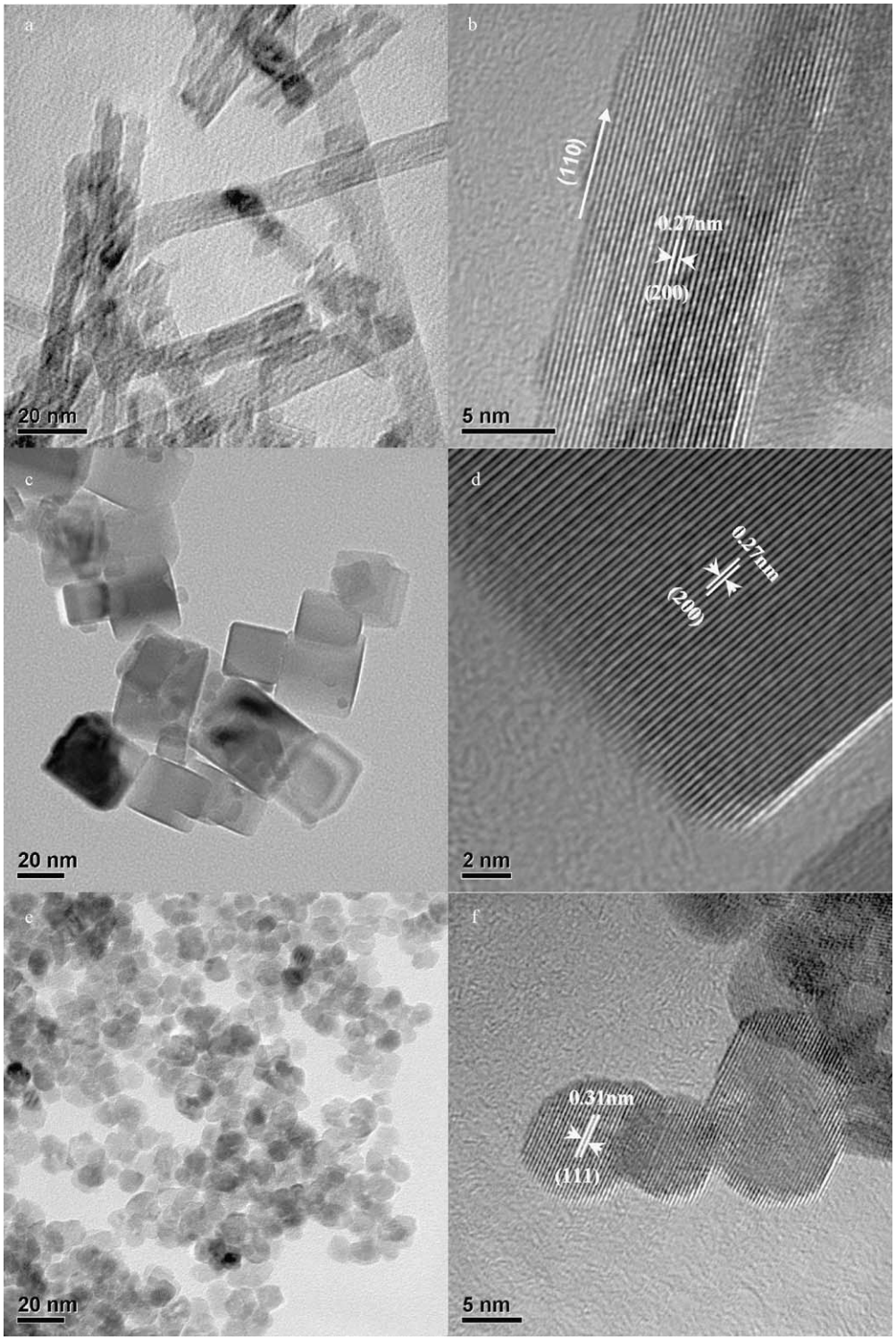

Fig. 2. TEM and HRTEM images of Au/CeO_2 catalysts with different CeO_2 shapes. (a) and (b): Au/CeO_2-rods; (c) and (d): Au/CeO_2-cubes; (e) and (f): Au/CeO_2-polyhedra.

At 363 K, the CO conversion over the catalyst of Au/CeO_2-rods was higher than 90%, whereas that over the Au/CeO_2-cubes was only about 30%. The activity sequence for these three samples in Fig. 1 was similar to the previous one obtained in the case of without CO_2 and H_2O moisture [24]. However, in comparison to the CO-PROX performance in the absence of CO_2 and H_2O, the result indicated that the co-existences of CO_2 and H_2O would show negative effects. Nevertheless, the CeO_2 crystalline shape dependence of Au/CeO_2 catalysts on the CO-PROX performance could be obtained either in the absence or presence of CO_2 and H_2O moisture.

To exclude the gold size effect, we have further measured the TEM and HRTEM images of the Au/CeO_2 catalysts with different CeO_2 shapes. As shown in Fig. 2, after gold deposition, the CeO_2 nanocrystals maintained their original shapes. The Au/CeO_2-nanorods showed a uniform width of approximate 10 nm with length 50–200 nm (Fig. 2a). The Au/CeO_2-nanocubes displayed an average size of about 25 nm (Fig. 2c) and the Au/CeO_2-nanopo-

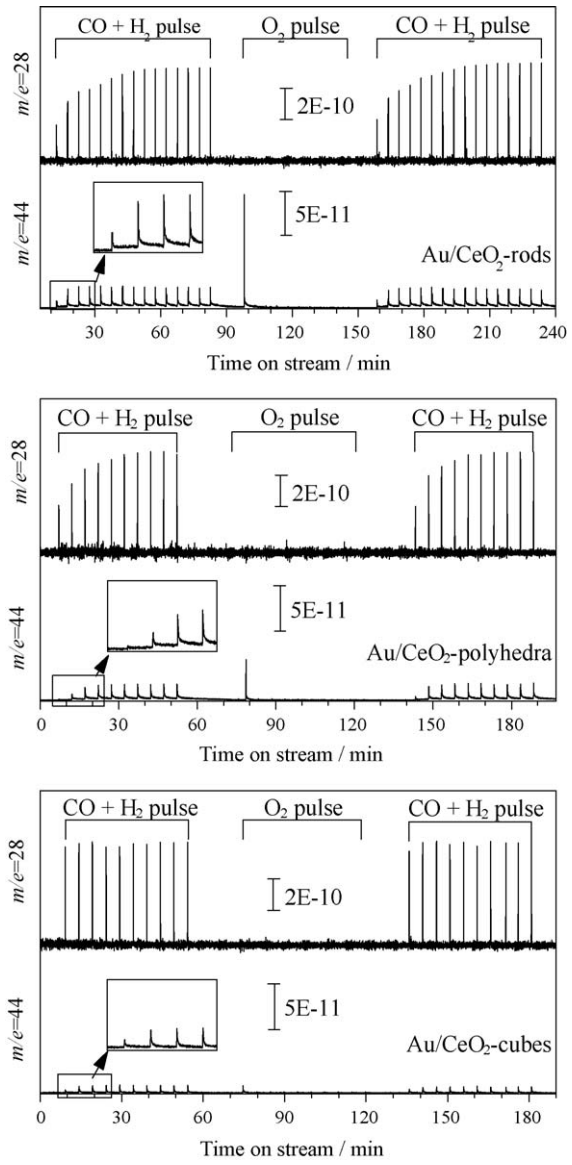

Fig. 3. Pulse reactions of CO–H_2 mixed gas and O_2 alone over Au/CeO_2 catalysts with different CeO_2 shapes at 323 K. The inserts refer to the magnified signal of m/e = 44 during the first pulse to the fourth pulse of CO–H_2 mixed gas.

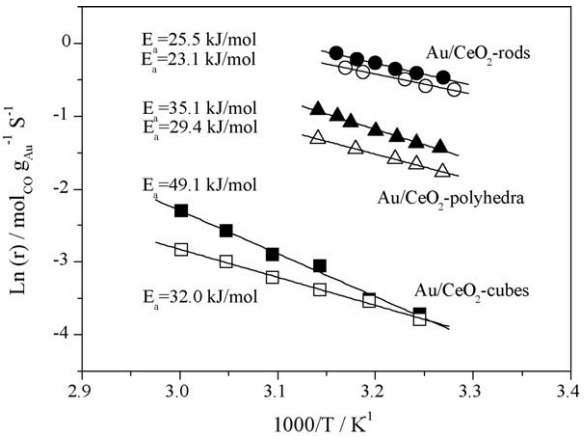

Fig. 4. Arrhenius plots of CO oxidation rates of Au/CeO_2 catalysts with different CeO_2 shapes for CO-PROX reaction (solid symbols) and CO oxidation in the absence of hydrogen (open symbols).

lyhedra had a diameter around 9 nm (Fig. 2e). The HRTEM images indicated that the exposed crystal planes of the Au/CeO_2-nanorods were dominated by {1 1 0} and {1 0 0} facets of CeO_2 (Fig. 2b), those of the Au/CeO_2-nanocubes and the Au/CeO_2-nanopolyhedra were done by {1 0 0} (Fig. 2d) and {1 1 1} (Fig. 2f), respectively [28]. It can be seen that the gold nanoparticles with diameters smaller than 3 nm were identified on the CeO_2-nanocubes, but those were hardly observed on other two shapes of CeO_2 nanocrystals due to the low contrast of Au. In combination with the XRD patterns and ICP analyses [24], we concluded that the highly dispersed gold clusters were evident on the Au/CeO_2 samples investigated. The weak contrast of Au particles might be possibly due to the diffusion of Au into bulk CeO_2 or the formation of Au–Ce alloy *via* oxygen vacancies [19,30]. These observations indicated there might exist stronger interactions between gold nanoparticles and CeO_2 nanocrystals, in particular, the CeO_2 with shapes of rods and polyhedra.

The results of O_2-TPD indicated that after deposition of gold significant O_2 desorptions were observed on the Au/CeO_2-rods and Au/CeO_2-polyhedra at 773–1173 K, but no O_2 species were released on Au/CeO_2-cubes even at the temperature up to 1273 K [24]. The different O_2-TPD profiles for the Au-supported samples might be assigned to the different oxygen storage capacity of CeO_2, which might have great impact on the reaction activity [23,31,32]. Thus, the pulse experiments were performed to elucidate this behavior. The pulse reactions of CO–H_2 mixed gas and O_2 alone over the Au/CeO_2 with different CeO_2 shapes at 323 K are displayed in Fig. 3. Two mass signals, one for CO_2 with m/e = 44 and another for CO with m/e = 28 were monitored. The CO signal increased gradually and reached maximal after the tenth CO–H_2 pulses for the Au/CeO_2-rods, the eighth ones for the Au/CeO_2-polyhedra and the second ones for the Au/CeO_2-cubes. The signal of m/e = 44 was detected immediately after the CO–H_2 pulse for all the samples, but the highest signal was observed on the Au/CeO_2-rods. Interestingly, the intensity of CO_2 signal increased at the first to the fourth CO–H_2 pulses, and then began to decrease. It might be owing to the adsorption/activation of CO on the catalyst surfaces. We have measured the carbon balance between CO adsorbed and CO_2 produced. It was found that the amount of CO adsorbed was much larger than that of CO consumed for the generation of CO_2. This was consistent with the previous finding that no matter what the CeO_2 shapes were, the Au/CeO_2 catalysts absorbed much more CO that O_2 according to the CO-TPD and O_2-TPD results [24]. After the CO–H_2 pulses were saturated, the samples were pulsed with O_2. The CO_2 signal was detected only at the first O_2 pulse and its intensity was ranked by the CeO_2 shapes as rods > polyhedra > cubes. In other words, the adsorbed CO could be readily reacted with O_2, implying that O_2 activation on the catalyst surfaces was quite quick. After the tenth O_2 pulse, CO–H_2 was pulsed into the catalyst bed once again, giving almost the same behavior as the fresh samples.

Arrhenius plots of CO oxidation rate (r) over the Au/CeO_2 catalysts with different shapes are shown in Fig. 4. The catalytic activity followed the order of CeO_2 shapes by rods > polyhedra > cubes for CO oxidation either with or without H_2. As common feature, the CO oxidation rate could be enhanced by H_2 no matter what the Au/CeO_2 shapes were used. The CO-PROX reaction over the Au/CeO_2 catalysts with CeO_2 shapes of rods, polyhedra and cubes showed the apparent activation energies (E_a) of 25.5, 35.1 and 49.1 kJ mol^{-1}, respectively. Clearly, the E_a values were of CeO_2 shape dependence. The variation of E_a value due to the Au/CeO_2 with different shapes could be essentially attributed to the distinctly different interactions between gold and CeO_2 as described above and previously [24], indicating that the rate-determining step of CO-PROX reaction on

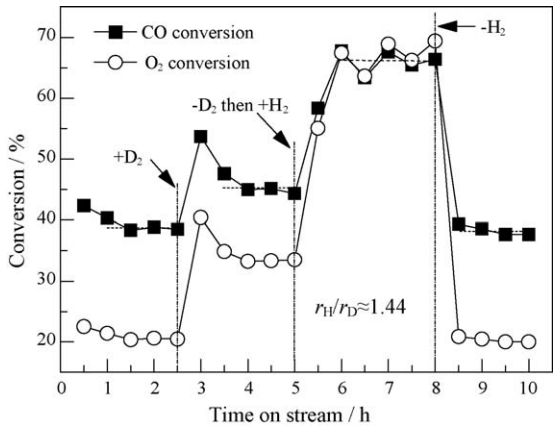

Fig. 5. The hydrogen isotope effect of CO oxidation activity over Au/CeO_2-cubes at 333 K. Total flow rate was 50 mL min^{-1}, where N_2 flow was lowered from 49 to 24 mL min^{-1} when a 25 mL min^{-1} of H_2 or D_2 gas was added.

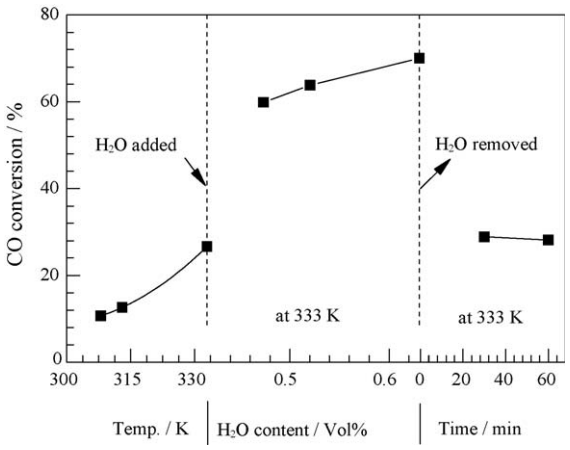

Fig. 6. The influence of H_2O content on the oxidation of CO over Au/CeO_2-cubes. H_2O pressure was controlled by adding dry N_2 to a flow of N_2 bubbled through a water tank at room temperature and monitored by the gas chromatograph.

the Au/CeO_2 catalysts with different shapes might be different from each other. A similar E_a sequence for CO oxidation without H_2 was also observed. The Au/CeO_2-rods exhibited the lowest apparent activation energy of 23.1 kJ mol^{-1}, while that for the Au/CeO_2-polyhedra and Au/CeO_2-cubes was 29.4 kJ mol^{-1} and 32.0 kJ mol^{-1}, respectively. Note, the CO oxidation in the CO-PROX showed higher E_a values in comparison with the CO oxidation without H_2. It is believably that the reaction mechanism of CO-PROX in H_2 would be different from the total oxidation of CO [26,27]. Moreover, it has been reported the H_2 oxidation, which could produce H-containing species that facilitate CO oxidation, usually showed a higher E_a value in the presence of CO [26]. Another possible interpretation of non-Arrhenius behavior of rate constant of the CO oxidation reaction is suggested in terms of the tunneling [33]. The highly active H-containing species might be also possibly generated through a quantum tunnel effect on the nanoscale Au/CeO_2 catalysts in the case of higher E_a value, resulting in a higher reaction rate for the CO-PROX.

To further clarify the mechanism of CO oxidation enhanced by H_2 on the Au/CeO_2 catalysts, we then performed the hydrogen isotope effect on the oxidation of CO. Since the CO oxidation on all the Au/CeO_2 catalysts showed similar promotional effect of H_2, only the result of Au/CeO_2-cubes was presented. As shown in Fig. 5, when D_2 (25 mL min^{-1}) was added to a flow of CO (0.5 mL min^{-1}) + O_2 (0.5 mL min^{-1}) + N_2 (49 mL min^{-1}) by lowering the N_2 to 24 mL min^{-1} at 333 K, the CO conversion was enhanced from 39.0% to 45.5%. When D_2 was replaced by H_2, the CO conversion further jumped to 65.5%. However, with the removal of H_2 from the stream, the CO conversion dropped the level of CO oxidation. The CO oxidation activity in the presence of H_2 was nearly 1.44 times of that in the presence of D_2. Interestingly, the O_2 conversion increased from 33.1% to 66.5% when D_2 was replaced by H_2, where the O_2 selectivity for CO oxidation was 68.7% in the presence of D_2 but 49.5% in the presence of H_2. This observed kinetic isotope effect (k_H/k_D = 1.44) implied that the step of activation of hydrogen or H-containing specie was involved in the CO-PROX reaction [34,35]. So it is reasonable to conclude that the H-containing species was responsible for the rate-determining step of CO-PROX. The hydrogen reacted with adsorbed oxygen to yield highly oxidizing surface intermediates that could readily convert CO to CO_2 at lower temperatures. One possible candidate of the H-containing species could be the OH group, which has been frequently mentioned in literature [27,36].

Fig. 6 shows the effect of H_2O moisture on the CO oxidation at 333 K. As can be seen, the conversion of CO was enhanced from 26.6% to 56.1% when a small amount of water vapor (0.47 vol%) was introduced to the feed gas and it was linearly increased with the increase of H_2O content. When the H_2O vapor was removed from the feed gas, the CO conversion was restored to the pristine level. It should be mentioned that too much water (5 vol% or more) was not beneficial for the CO oxidation at 333 K, probably because higher concentrations of H_2O led to the blocking of the active sites and thus hindered the adsorption of CO and O_2 [37]. It has been reported that the CO oxidation was enhanced by water on Au catalysts supported on Al_2O_3 and SiO_2 [38]. They explained that water promoted the CO oxidation by facilitating the activation of O_2. While in the present case, the CeO_2 support can easily adsorbed and activated oxygen, which made the promotional effect of H_2O on the Au/CeO_2 catalyst a little different. Based on the hydrogen effect and the above experimental results, we considered that H_2O promoted the CO oxidation by generating the OH group which accelerated the CO oxidation reaction.

4. Conclusion

In summary, the catalytic activity of Au/CeO_2 catalysts prepared by DP method with CeO_2 shapes of rods, cubes and polyhedra showed a strong morphology effect in the CO-PROX reaction. The Au/CeO_2-rods exhibited the lowest apparent activation energy and highest activity. The reaction was promoted by the existence of hydrogen or water vapor in the feed gas and indicated a hydrogen isotope effect by H_2/D_2. The results suggested that the mechanism of CO-PROX reaction over Au/CeO_2 might be different from ordinary oxidation of CO with oxygen alone. We proposed that hydrogen reacted with adsorbed oxygen to yield highly oxidizing surface H-containing intermediates that could readily converted CO to CO_2 at lower temperatures. The generation of such key intermediates might be involved into the rate-determining step.

Acknowledgements

We acknowledge financial supports from the NSFC (20433030 and 20873108), the 973 program (2009CB939804) and the Key Scientific Project of Fujian Province (2009HZ0002-1)

References

[1] B.C.H. Steele, A. Heinzel, Nature 414 (2001) 345.
[2] C.D. Dudfield, R. Chen, P.L. Adock, Int. J. Hydrogen Energy 26 (2001) 763.
[3] M. Shou, K. Tanaka, K. Yoshioka, Y. Moro-oka, S. Nagano, Catal. Today 90 (2004) 255.
[4] H.P. Dhar, L.G. Christner, A.K. Kush, J. Electrochem. Soc. 134 (1987) 3021.
[5] D.L. Trimm, Appl. Catal. A: Gen. 296 (2005) 1.
[6] E.D. Park, D. Lee, H.C. Lee, Catal. Today 139 (2009) 280.

[7] S. Carrettin, P. Concepcion, A. Corma, J.M.L. Nieto, V.F. Puntes, Angew. Chem. Int. Ed. 43 (2004) 2538.
[8] K. Tanaka, M. Shou, H.B. Zhang, Y.Z. Yuan, T. Hagiwara, A. Fukuoka, J. Nakamura, D.L. Lu, Catal. Lett. 126 (2008) 89.
[9] P.V. Snytnikov, V.A. Sobyanin, V.D. Belyaev, P.G. Tsyrulnikov, N.B. Shitova, D.A. Shlyapin, Appl. Catal. A: Gen. 239 (2003) 149.
[10] Y.Q. Huang, A.Q. Wang, L. Li, X.D. Wang, D.S. Su, T. Zhang, J. Catal. 255 (2008) 144.
[11] G. Avgouropoulos, T. Ioannides, Ch. Papadopoulou, J. Batista, S. Hocevar, H. Matralis, Catal. Today 75 (2002) 157.
[12] M.M. Schubert, A. Venugopal, M.J. Kahlich, V. Plzak, R.J. Behm, J. Catal. 222 (2004) 32.
[13] W. Deng, J. De Jesus, H. Saltsburg, M. Flytzani-Stephanopoulos, Appl. Catal. A: Gen. 291 (2005) 126.
[14] W.Y. Yu, C.P. Yang, J.N. Lin, C.N. Kuo, B.Z. Wan, Chem. Commun. (2005) 354.
[15] H. Imai, M. Date, S. Tsubota, Catal. Lett. 124 (2008) 68.
[16] L.H. Chang, Y.L. Yeh, Y.W. Chen, Int. J. Hydrogen Energy 33 (2008) 1965.
[17] W.S. Shin, C.R. Jung, J. Han, S.W. Nam, T.H. Lim, S.A. Hong, H.I. Lee, J. Ind. Eng. Chem. 10 (2004) 302.
[18] M. Manzoli, G. Avgouropoulos, T. Tabakova, J. Papavasiliou, T. Ioannides, F. Boccuzzi, Catal. Today 138 (2008) 239.
[19] F. Arena, P. Famulari, G. Trunfio, G. Bonura, F. Frusteri, L. Spadaro, Appl. Catal. B: Environ. 66 (2006) 81.
[20] W. Deng, C. Carpenter, N. Yi, M. Flytzani-Stephanopoulos, Top. Catal. 44 (2007) 199.
[21] A.A. Herzing, C.J. Kiely, A.F. Carley, P. Landon, G.J. Hutchings, Science 321 (2008) 1331.
[22] F. Romero-Sarria, A. Penkova, L.M. Martinez, M.A. Centeno, K. Hadjiivanov, J.A. Odriozola, Appl. Catal. B: Environ. 84 (2008) 119.
[23] A. Trovarelli, Catal. Rev. Sci. Eng. 38 (1996) 439.
[24] G.Q. Yi, Z.N. Xu, G.C. Guo, K. Tanaka, Y.Z. Yuan, Chem. Phys. Lett. 479 (2009) 128.
[25] M. Haruta, S. Tsubota, T. Kobayashi, H. Kageyama, M.J. Genet, B. Delmon, J. Catal. 144 (1993) 175.
[26] E. Quinet, F. Morfin, F. Diehl, P. Avenier, V. Caps, J.L. Rousset, Appl. Catal. B: Environ. 80 (2008) 195.
[27] K. Tanaka, M. Shou, H. He, X. Shi, X. Zhang, J. Phys. Chem. C 113 (2009) 12427.
[28] H.X. Mai, L.D. Sun, Y.W. Zhang, R. Si, W. Feng, H.P. Zhang, H.C. Liu, C.H. Yan, J. Phys. Chem. B 109 (2005) 24380.
[29] R. Si, M. Flytzani-Stephanopoulos, Angew. Chem. Int. Ed. 47 (2008) 2884.
[30] T. Akita, M. Okumura, K. Tanaka, M. Kohyama, M. Haruta, Catal. Today 117 (2006) 62.
[31] Z.X. Yang, T.K. Woo, K. Hermansson, Chem. Phys. Lett. 396 (2004) 384.
[32] D.C. Sayle, S.A. Maicaneanu, G.W. Watson, J. Am. Chem. Soc. 124 (2002) 11429.
[33] E.D. German, M. Sheintuch, J. Phys. Chem. C 111 (2007) 9184.
[34] C.K. Costello, J.H. Yang, H.Y. Law, Y. Wang, J.-N. Lin, L.D. Marks, M.C. Kung, H.H. Kung, Appl. Catal. A 243 (2003) 15.
[35] H.H. Kung, M.C. Kung, C.K. Costello, J. Catal. 216 (2003) 425.
[36] M. Kuriyama, H. Tanaka, S. Ito, T. Kubota, T. Miyao, S. Naito, K. Tomishige, K. Kunimori, J. Catal. 252 (2007) 39.
[37] M. Date, M. Haruta, J. Catal. 201 (2001) 221.
[38] M. Date, M. Okumura, S. Tsubota, M. Haruta, Angew. Chem. Int. Ed. 43 (2004) 2129.